VOLUME 115, NUMBER 6
MARCH 24, 1993

JOURNAL
OF THE
AMERICAN
CHEMICAL
SOCIETY

Crystal Structure and Electron Spin Echo Envelope Modulation Study of [Cu(II)(TEPA)(NO_2)]PF_6 (TEPA = Tris[2-(2-pyridyl)ethyl]amine): A Model for the Purported Structure of the Nitrite Derivative of Hemocyanin

Feng Jiang,*,† Rebecca R. Conry,‡ Luigi Bubacco,§ Zoltán Tyeklár,‡ Richard R. Jacobson,‡ Kenneth D. Karlin,‡ and Jack Peisach†,§

Contribution from the Department of Molecular Pharmacology and Department of Physiology and Biophysics, Albert Einstein College of Medicine of Yeshiva University, Bronx, New York 10461, and Department of Chemistry, The Johns Hopkins University, Baltimore, Maryland 21218. *Received September 25, 1992*

Abstract: The coordination properties of nitrite ion (NO_2^-) with copper are relevant to investigations of a variety of copper proteins, including those involved in nitrogen oxide processing. Here, we use X-ray diffraction and electron spin echo envelope modulation (ESEEM) spectroscopy to investigate the coordination and electronic structure of a nitrite–copper(II) model compound, [Cu(II)(TEPA)NO_2]PF_6 (TEPA = tris[2-(2-pyridyl)ethyl]amine). In the crystal ($C_{21}H_{24}N_5CuO_2PF_6$ crystallizes in the monoclinic space group $P2_1/c$ with $Z = 4$, $a = 11.817(8)$ Å, $b = 13.124(6)$ Å, $c = 15.692(7)$ Å, and $\beta = 92.39(4)°$), nitrite is shown to bind as an equatorial ligand to Cu(II) through oxygen, rather than nitrogen. In frozen solution, the detection of ESEEM from the nitrite ^{14}N indicates O-ligation as well. The quadrupole and electron–nuclear coupling tensors for the nitrite ^{14}N are obtained by field-dependent ESEEM spectral simulation. The quadrupole parameters, $e^2qQ = 5.66$ MHz and $\eta = 0.31$, are similar to those for diamagnetic metal nitrites. The net charge on the nitrite nitrogen calculated from the quadrupole parameters, based on Townes–Dailey theory, suggests that the ONO angle of bound nitrite is between 111° and 116° in frozen solution, as compared to 115° in the crystal. The principal directions of the quadrupole tensor and the electron–nuclear coupling tensor relative to that of the **g** tensor suggest that the ONO orientation relative to the Cu(II)(TEPA) structure in frozen solution is essentially the same as that in the crystal. The ability to observe modulations arising from Cu(II)-coordinated $^{14}NO_2^-$ allows us to probe for an equatorial nitrito ligand to Cu(II) in solution samples. An attempt was made to substantiate the claim that nitrite binds equatorially through oxygen to Cu(II) in hemocyanin after nitrite treatment (Solomon, E. I. In *Copper Proteins*; Spiro, T. G., Ed.; Wiley-Interscience: New York, 1981; pp 43–108) by searching for $^{14}NO_2^-$ modulations in the ESEEM spectrum. None were found, suggesting that nitrite does not coordinate to the Cu(II) of hemocyanin as claimed.

Introduction[1]

Cu–NO_x complexes are relevant in the study of copper-containing enzymes involved in the denitrification process,[2] i.e., the bacterial dissimilatory reduction of nitrate and nitrite to NO, N_2O, and N_2. In particular, copper–nitrite complexes are potentially relevant to the nitrite reductases[3] which convert NO_2^- to NO

* To whom correspondence should be addressed.
† Department of Molecular Pharmacology, Albert Einstein College of Medicine of Yeshiva University.
‡ The Johns Hopkins University.
§ Department of Physiology and Biophysics, Albert Einstein College of Medicine of Yeshiva University.

(1) Abbreviations: ESEEM, electron spin echo envelope modulation; TEPA, tris[2-(2-pyridyl)ethyl]amine; NQI, nuclear quadrupole interaction; NQR, nuclear quadrupole resonance; efg, electric field gradient; CW, continuous wave; bpy, 2,2′-bipyridyl; terpy, terpyridine; HB(^{t}Bu-pz)$_3$, hydrotris(3-*tert*-butylpyrazolyl)borate anion.

(2) (a) Kroneck, M. H.; Zumft, W. G. In *Denitrification in Soil and Sediment*; Revsbech, N. P., Sørensen, J., Eds.; FEMS Symposium 56; Academic: London, 1990; pp 1–20. (b) Hochstein, L. I.; Tomlinson, G. A. *Annu. Rev. Microbiol.* **1988**, *42*, 231–261. (c) Knowles, R. *Microbiol. Rev.* **1982**, *46*, 43–70. (d) Averill, B. A.; Tiedje, J. M. *FEBS Lett.* **1982**, *138*, 8–12.

0002-7863/93/1515-2093$04.00/0

and/or N_2O, reactions presumed to proceed by nitrite binding to Cu(II), followed by dehydration and reduction. In addition, small molecules such as nitrite have been used as spectroscopic and reactivity probes of the active sites of metalloenzymes, an example being the studies involving NO and NO_2^- with hemocyanin; both of these reagents produce the same product, which has been proposed to be a copper(II)–nitrite complex,[4] although this has been questioned.[5]

The coordination of a metal ion to nitrite can, in theory, occur either through oxygen or nitrogen. Although X-ray data can be used to unequivocally make a structural assignment for the crystalline sample, structural assignment for solution samples is more difficult. One can, however, make an assignment from the nitrite-^{14}N quadrupole parameters, e^2qQ and η, which are determined by the electron population in the valence-shell orbitals.[6] Such measurements have been carried out using nuclear quadrupole resonance spectroscopy, but only for solid samples. In the presence of a paramagnetic metal ion, ESEEM[1] spectroscopy can be applied to obtain the quadrupole parameters of metal-bound quadrupolar nuclei in solution. Under favorable conditions, it is possible to determine e^2qQ and η, as well as the orientation of the quadrupole tensor with respect to a structural feature, as in this study, where we have been able to make a determination of the structure of a metal–nitrite complex.

In this investigation we have studied the structure of a copper(II)–nitrite complex with a polydentate nitrogenous ligand, [Cu(II)(TEPA)(NO_2)]PF_6, both in the crystalline form by X-ray diffraction and in frozen solution by ESEEM spectroscopy. For the first time we have been able to identify the ESEEM arising from Cu(II)-coordinated $^{14}NO_2^-$, demonstrating that it is possible to use ESEEM spectroscopy to probe $^{14}NO_2^-$ binding to Cu(II). From the simulation of field-dependent ESEEM spectra, we were able to determine the superhyperfine parameters, including the nuclear quadrupole parameters and the electron–nuclear coupling constants, as well as the directions of the principal axes of the quadrupole tensor and the electron–nuclear coupling tensor relative to that of the **g** tensor. Because the principal direction of the three tensors are related to the symmetry axis of the molecule, we were able to compare the structure of Cu(II)-coordinated nitrite in solution with that in the crystal. It was found that in both states nitrite binds to Cu(II)(TEPA) through oxygen with similar ONO orientation and ONO bond angle.

Since nitrite binding to Cu(II) can be recognized by ESEEM spectroscopy, an attempt was made to demonstrate the presence of nitrite as an equatorial nitrito ligand on Cu(II) in nitrite-treated hemocyanin, as suggested by Solomon and co-workers.[4a] Although we can clearly identify and differentiate [^{14}N]nitrite and [^{15}N]-nitrite in ESEEM spectra for the model compound [Cu(II)-(TEPA)(NO_2)]PF_6, no difference that could be attributed to nitrite is observed in ESEEM spectra for the protein. We conclude, then, that either nitrite is not bound to the hemocyanin Cu(II) in the nitrite-treated protein or that it is coordinated in a manner which is substantially different from that in the model.

Experimental Section

Synthesis of Model Complexes. [Cu(II)(TEPA)(NO_2)]PF_6 (**1**) was generated from [Cu(II)(TEPA)(Cl)]PF_6 (**2**)[7-10] as follows. Compound **1** (0.50 g, 0.87 mmol) was dissolved in a mixture of 50 mL of MeOH and 10 mL of CH_3CN, then $NaNO_2$ (0.061 g, 0.87 mmol) was added as a solid. The blue color of the solution immediately changed to deep green. The mixture was stirred for 1 h, and the solvent was removed by rotary evaporation. The resulting green residue was dissolved in CH_2Cl_2 (75 mL), filtered, and layered with Et_2O (ca. 150 mL). After 4 days, the green crystals produced were collected by decantation of the solvent and dried in air, giving 0.34 g (54%) of **1**·$^1/_2CH_2Cl_2$. Anal. Calcd for $C_{21.5}H_{25}ClCuF_6N_5O_2P$: C, 41.03; H, 4.00; N, 11.13. Found: C, 41.14; H, 3.94; N, 11.24. The presence of $^1/_2CH_2Cl_2$ solvate was confirmed by reduction (KCN in CD_3CN) of **1**·$^1/_2CH_2Cl_2$ followed by ^{1}H NMR spectroscopic analysis. The ^{15}N-labeled derivative of **1** was prepared similarly using $Na^{15}NO_2$ (99%, Icon Services, Inc.).

X-ray Diffraction. The blue-green crystals of **1** were grown by vapor diffusion of Et_2O into a methanolic solution of **1** at ambient temperature. A summary of the crystal data is given in Table I, selected bond lengths and angles are given in Table II, and selected atomic coordinates are

Table I. Crystallographic Data for [Cu(II)(TEPA)(NO_2)]PF_6

formula	$C_{21}H_{34}N_5CuO_2PF_6$
formula weight	586.96
crystal system	monoclinic
space group	$P2_1/c$ (#14)
a, Å	11.817(8)
b, Å	13.124(6)
c, Å	15.692(7)
β, deg	92.39(4)
V, Å^3	2432(2)
Z	4
temperature, K	298
ρ_{calcd}, g/cm^3	1.60
$\mu_{(MoK\alpha)}$, cm^{-1}	10.37
radiation (λ, Å)	0.71069
reflections collected	4722
independent reflections	1938 ($\geq 3\sigma\|F_o\|$)
no. of refined parameters	325
largest peak/hole, e Å^{-3}	0.34/−0.26
R^a	0.039
R_w^b	0.044
goodness of fit	1.98

$^a R = \sum||F_o| - |F_c||/\sum|F_o|$. $^b R_w = [\sum w(|F_o| - |F_c|)^2/\sum wF_o^2]^{1/2}$.

Table II. Selected Distances and Angles for [Cu(II)(TEPA)(NO_2)]PF_6

atom	distance, Å	atom	angle, deg
Cu–O(1)	2.012(5)	O(1)–N(5)–O(2)	114.9(7)
Cu–N(1)	2.083(5)	O(1)–Cu–N(1)	166.9(2)
Cu–N(2)	2.039(5)	O(1)–Cu–N(2)	87.8(2)
Cu–N(3)	2.049(5)	O(1)–Cu–N(3)	86.7(2)
Cu–N(4)	2.253(5)	O(1)–Cu–N(4)	94.6(2)
		N(1)–Cu–N(2)	94.1(2)
O(1)–N(5)	1.279(8)	N(1)–Cu–N(3)	89.4(2)
O(2)–N(5)	1.219(8)	N(1)–Cu–N(4)	98.2(2)
		N(2)–Cu–N(3)	170.1(2)
O(2)–Cu	2.633(6)	N(2)–Cu–N(4)	94.8(2)
N(5)–Cu	2.746(7)	N(3)–Cu–N(4)	93.9(2)

Table III. Selected Positional Coordinates for [Cu(II)(TEPA)(NO_2)]PF_6

atom	x	y	z	B(eq)
Cu	0.67122(6)	0.12705(6)	0.36737(5)	3.65(4)
O(1)	0.5526(5)	0.0186(4)	0.3792(3)	5.4(3)
O(2)	0.4882(5)	0.0950(5)	0.2696(4)	8.3(4)
N(1)	0.7654(4)	0.2554(4)	0.3375(3)	4.0(3)
N(2)	0.7402(4)	0.0383(4)	0.2763(3)	4.1(3)
N(3)	0.5768(4)	0.2147(4)	0.4457(3)	3.8(3)
N(4)	0.7848(5)	0.0674(4)	0.4750(3)	4.4(3)
N(5)	0.4758(6)	0.0252(6)	0.3196(5)	7.2(3)

(3) (a) Ye, R. W.; Toro-Suarez, I.; Tiedjie, J. M.; Averill, B. A. *J. Biol. Chem.* **1991**, *266*, 12848–12851. (b) Bryan, B. A.; Shearer, G.; Sketters, J. L.; Kohl, D. H. *J. Biol. Chem.* **1983**, *258*, 8613–8617. (c) Godden, J. W.; Turley, S.; Teller, K. C.; Adman, E. T.; Liu, M. Y.; Payne, W. J.; Legall, J. *Science* **1991**, *253*, 438–442. (d) Garber, E. A. E.; Wehrlik, S.; Hollocher, T. C. *J. Biol. Chem.* **1983**, *258*, 3587–3591. (e) Tiedje, J. M.; Averill, B. A. *FEBS Lett.* **1991**, *291*, 41–44.

(4) (a) Himmerlwright, R. S.; Eickman, N. C.; Solomon, E. I. *Biochem. Biophys. Res. Commun.* **1978**, *81*, 237–242. (b) Solomon, E. I. In *Copper Proteins*; Spiro, T. G., Ed.; Wiley-Interscience: New York, 1981; pp 43–108.

(5) (a) Salvato, B.; Giacometti, G. M.; Beltramini, M.; Zilio, F.; Giacometti, G.; Magliozzo, R. S.; Peisach, J. *Biochemistry* **1989**, *28*, 680–684. (b) Tahon, J.-P.; Van Hoof, D.; Vinckier, C.; Witters, R.; De Ley, M.; Lontie, R. *Biochem. J.* **1981**, *249*, 891–896.

(6) Townes, C. H.; Dailey, B. P. *J. Chem. Phys.* **1949**, 782–796.

(7) Jacobson, R. R. Ph.D. Dissertation, State University of New York (SUNY) at Albany, 1989.

(8) Zubieta, J.; Karlin, K. D.; Hayes, J. C. In *Copper Coordination Chemistry: Biochemical and Inorganic Perspectives*; Karlin, K. D., Zubieta, J., Eds.; Adenine: Guilderland, NY, 1983; pp 97–108.

(9) Karlin, K. D.; Hayes, J. C.; Juen, S.; Hutchinson, J. P.; Zubieta, J. *Inorg. Chem.* **1982**, *21*, 4106–4108.

(10) Karlin, K. D.; Dahlstrom, P. L.; Hayes, J. C.; Simon, R. A.; Zubieta, J. *Cryst. Struct. Commun.* **1982**, *11*, 907–912.

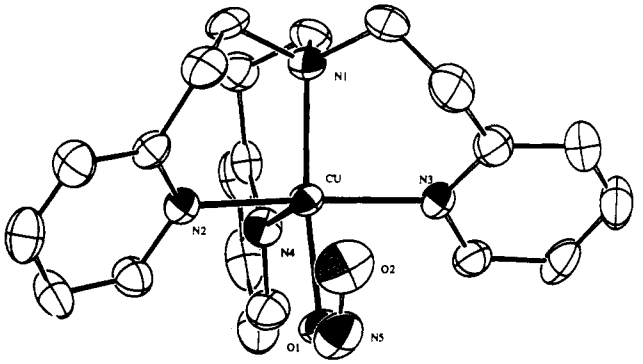

Figure 1. ORTEP drawing of the cationic portion of **1** with 30% probability ellipsoids.

given in Table III. All calculations were performed using the TEXSAN crystallographic software package.[11]

Spectroscopy. Infrared spectra were recorded as KBr pellets on a Mattson Galaxy 4030 FT-IR spectrometer.

Samples for magnetic resonance investigation were prepared by dissolving crystals of **1** in CH_2Cl_2. In order to form a good glass, an equal volume of toluene was added so that the final concentration of Cu(II) was 1 mM. Continuous-wave EPR investigations of **1** and of the EPR-active forms of hemocyanin were carried out at 77 K on a Varian E-112 spectrometer equipped with a Systron-Donner frequency counter and a Varian NMR gaussmeter. Spectral simulations were carried out with a program supplied by L. Belford and described by Nilges[12] and Maurice.[13]

Electron spin echo envelopes were obtained on a home-built pulsed EPR spectrometer, described previously,[14] using a folded stripline cavity[15] which is compatible with conventional 4 mm o.d. EPR tubes. Data were collected at 4.2 K using either two-pulse (90°-τ-180°) or three-pulse (90°-τ-90°-T-90°) procedures.[16] Three-pulse data were obtained with the time τ, the spacing between the first two microwave pulses, equal to integer multiples of the proton periodicity in order to suppress modulations arising from weakly coupled protons.[16c] Typical measurement conditions were the following: microwave frequency, 8.8 GHz; magnetic field strength, 3100 G; microwave power, 45 W; pulse width, 20 ns; sample temperature, 4.2 K; pulse repetition rate, 100 Hz. Fourier transformation of three-pulse data was carried out subsequent to dead-time reconstruction according to the method of Mims.[17] The identification of lines arising from $^{14}NO_2^-$ in the ESEEM spectrum of **1** was achieved by comparing spectra of complexes prepared with [^{15}N]- and [^{14}N]nitrite.

Field-dependent ESEEM spectral simulations of three-pulse modulation data obtained at six magnetic field settings across the EPR absorption envelope were obtained by using the density matrix formalism of Mims,[18] together with an averaging scheme developed for angle-selected ENDOR.[19] For a frozen solution sample, the EPR spectrum reflects a "powder" average of all molecular orientations with respect to the magnetic field. When the CW EPR spectrum is dominated by the g and metal nuclear hyperfine anisotropy, only a specific set of molecular orientations is excited at a given magnetic field. A molecular orientation is described by the polar angles, θ and ϕ, relating the orientation of the magnetic field with respect to the principal axis of the **g** tensor. They are determined by the excitation frequency, nuclear spin quantum number, and principal values of g and metal hyperfine tensors (eq 2 of ref 20). Because the ESEEM measurement is performed at a constant magnetic field setting within the EPR absorption, with the 20-ns microwave pulses used, molecules resonating at about 9 G at each side of the magnetic field setting contribute to the spin echo observed. In our field-dependent ESEEM simulations, the orientations of molecules on resonance are first determined iteratively by searching for θ when ϕ is stepped from 0° to 360°, and the modulation functions calculated for each pair of θ and ϕ are summed to give the simulated echo envelope.[21]

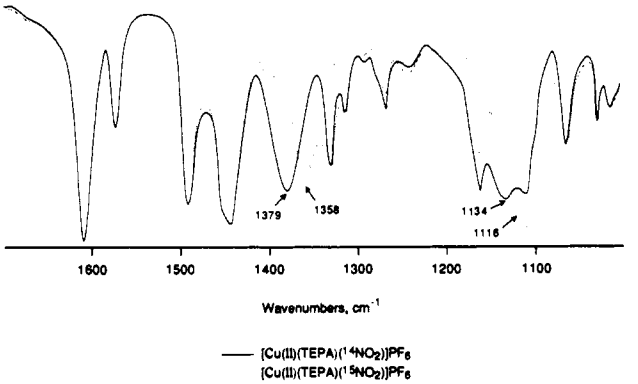

Figure 2. Infrared spectra of **1**: solid line, prepared with $^{14}NO_2$; dashed line, prepared with $^{15}NO_2$.

Preparation of Protein Samples. *Octopus vulgaris* hemocyanin[22] (1-2 mM) in 50 mM phosphate buffer, pH 5.5, was treated for 20 h with 5 mM [^{14}N]- or [^{15}N]nitrite in the presence of 5 mM ascorbate. Excess reagents were removed by extensive dialysis. Protein samples used for spectroscopic examination were concentrated by pressure filtration to a final Cu(II) concentration of about 1 mM. The protein products of the nitrite reactions were characterized as before from their EPR and optical spectral properties.[5a]

Results and Discussion

Description of the Structure. The structure of [Cu(II)(TEPA)(NO$_2$)]$^+$ in the crystalline state is depicted in Figure 1. Like other Cu(II)(TEPA) derivatives,[7-10] **1** has a distorted square pyramidal geometry, with one of the pyridyl nitrogens, N(4), at the apical position. Nitrite coordinates to Cu(II) through oxygen (Cu-O(1) = 2.012(5) Å), trans to the amino nitrogen. The nitrito oxygen, the amino nitrogen, and the other two pyridyl nitrogens form an equatorial plane encompassing Cu(II).

Three nitrite binding conformations have been observed for mononuclear Cu(II) structures. In [Cu(terpy)(NO$_2$)OH$_2$]$^+$,[23] nitrite binds to copper with only one oxygen (nitrito); in Cu(bpy)(NO$_2$)$_2$[24a] and [Cu(bpy)$_2$(NO$_2$)]$^+$,[24b] nitrite binds through both oxygens; in [Cu(NO$_2$)$_6$]$^{4-}$,[25] nitrite is bound to nitrogen (nitro); and for K$_3$[Cu(NO$_2$)$_5$],[26] surprisingly, all three modes are seen. In **1**, the binding of nitrite is primarily through one of the oxygens.

There may be some interaction between the copper and the second nitrite oxygen (Cu···O(2) = 2.633(6) Å) (Figure 1), which contributes to lengthening of the 'trans' Cu-N(4) bond; 2.253(5) Å, as compared to 2.209 Å av for other Cu(II)(TEPA) complexes.[8] This interaction is obviously much weaker than that of Cu-O(1) so that the two N-O bonds are inequivalent. The strong binding

(11) TEXSAN-TEXRAY Structure Analysis Package, Molecular Structure Corporation, 1985.
(12) Nilges, M. J. Ph.D. Thesis, University of Illinois, Urbana, IL, 1979.
(13) Maurice, A. M. Ph.D. Thesis, University of Illinois, Urbana, IL, 1981.
(14) McCracken, J.; Peisach, J.; Dooley, D. M. *J. Am. Chem. Soc.* **1987**, *109*, 4064-4072.
(15) (a) Lin, C. P.; Bowman, M. K.; Norris, J. R. *J. Magn. Reson.* **1985**, *65*, 369-374. (b) Britt, R. D.; Klein, M. P. *J. Magn. Reson.* **1987**, *74*, 533-540.
(16) (a) Hahn, E. L. *Phys. Rev.* **1950**, *80*, 580-594. (b) Peisach, J.; Mims, W. B.; Davis, J. L. *J. Biol. Chem.* **1979**, *254*, 12379-12389. (c) Mims, W. B.; Peisach, J. In *Biological Magnetic Resonance*; Berliner, L. J., Reuben, J., Eds.; Plenum: New York, 1981; Vol. 3, pp 213-263.
(17) Mims, W. B. *J. Magn. Reson.* **1984**, *59*, 291-306.
(18) Mims, W. B. *Phys. Rev.* **1972**, *5*, 2409-2419.
(19) (a) Hurst, G. C.; Henderson, T. A.; Kreilick, R. W. *J. Am. Chem. Soc.* **1985**, *107*, 580-594. (b) Henderson, T. A.; Hurst, G. C.; Kreilick, R. W. *J. Am. Chem. Soc.* **1985**, *107*, 7299-7303.
(20) Cornelius, J. B.; McCracken, J.; Clarkson, R. B.; Belford, R. L.; Peisach, J. *J. Phys. Chem.* **1990**, *94*, 6977-6982.
(21) In the determination of θ and ϕ that satisfy the resonant condition, only g and metal hyperfine anisotropy are considered. Weaker interactions, e.g. metal quadrupole and ligand hyperfine, are treated by applying a lineshape function with a field width, rather than including them in the orientation selection process.[20]
(22) Salvato, B.; Ghiretti-Magaldi, A.; Ghiretti, F. *Biochemistry* **1979**, *18*, 27-37.
(23) Allmann, R.; Kremer, S.; Jucharzcyk, D. *Inorg. Chim. Acta* **1985**, *85*, L19-L21.
(24) (a) Stephens, F. S. *J. Chem. Soc., A* **1969**, 2081-2087. (b) Walsh, A.; Walsh, B.; Murphy, B.; Hathaway, B. J. *Acta Crystallogr.* **1981**, *B37*, 1512-1520.
(25) (a) X-ray structures: Takagi, S.; Joesten, M. D.; Lenhert, P. G. *J. Am. Chem. Soc.* **1975**, *97*, 444-445. Cullen, D. L.; Lingafelter, E. C. *Inorg. Chem.* **1971**, *10*, 1264-1268. (b) Powder neutron diffraction studies: Klein, S.; Reinen, D. *J. Solid State Chem.* **1980**, *32*, 311-319 and references therein.
(26) Klanderman, K. A.; Hamillton, W. C.; Bernal, I. *Inorg. Chim. Acta* **1977**, *23*, 117-129.

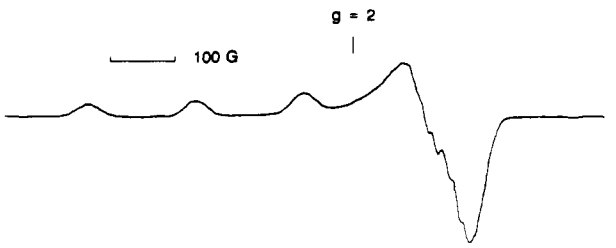

Figure 3. Continuous wave EPR spectrum of 1. Experimental conditions: microwave frequency, 9.090 GHz; microwave power, 5 mW; temperature, 77 K; modulation amplitude, 5.0 G; modulation frequency, 100 KHz.

of Cu(II) to O(1) lengthens the N(5)–O(1) bond by 0.06 Å as compared to the N(5)–O(2) bond.

The nitrite ONO angle observed for Cu(II)–NO_2 complexes[23-26] varies between 110° and 125°. The angle O(1)–N(5)–O(2) obtained for our model complex, 114.9(7)°, is well within this range.

Infrared Spectroscopy. The infrared spectrum of [Cu(II)(TEPA)($^{14}NO_2$)]PF_6 (Figure 2) contains prominent peaks at 1134 and 1379 cm^{-1}, which shift to 1116 (sh) and 1358 cm^{-1} for the same complex prepared with $^{15}NO_2^-$. Thus, these absorptions are attributed to the metal-bound ligand, nitrite.

For mononuclear metal nitrite complexes, the infrared spectrum is indicative of the type of structure formed. The pattern in Figure 2 is typical for an oxygen-bound nitrite group, most likely as a monodentate ligand [ν(N=O) 1485–1400 cm^{-1} and ν(N—O) 1110–1050 cm^{-1}].[27] But it is also possible that there is a weak interaction between Cu(II) and the second nitrite O-atom (e.g. Cu–O > 2.4 Å), since the IR pattern and frequencies very closely match those of Cu(II)(bpy)(NO_2)$_2$, where there is a weak interaction between Cu(II) and the second oxygen (Cu–O = 1.99 Å and Cu–O = 2.49 Å).[24a] Symmetrical bidentate oxygen-bound nitrite metal complexes, including that observed recently in the structurally characterized complex [HB(^{t}Bu-pz)$_3$]Cu(NO_2),[28] exhibit absorptions in different frequency ranges. A nitro complex, with direct nitrogen coordination (ν_{as} 1470–1370 cm^{-1} and ν_s 1340–1420 cm^{-1}), can be ruled out by the IR spectrum, consistent with the X-ray diffraction study.

EPR Spectroscopy. The typical axial CW EPR spectrum of 1 (Figure 3) suggests a $d_{x^2-y^2}$ ground state for Cu(II), consistent with the square pyramidal Cu(II) geometry. On the basis of spectral simulation,[29] $g_\parallel$ = 2.249, $g_\perp$ = 2.050, $A_\parallel$ = 527 MHz, and $A_\perp$ = ~47 MHz. No difference in the CW EPR is seen when either [^{14}N]- or [^{15}N]nitrite is coordinated, and none is expected (see below).

ESEEM Spectroscopy. Electromagnetic couplings between the unpaired electron of Cu(II) and an ^{14}N nucleus are a consequence of the nuclear Zeeman, the electron–nuclear hyperfine, and the nuclear quadrupole interactions. The spin Hamiltonian for ^{14}N is given by eq 1.

$$\mathcal{H}_N = -g_N\beta_N\mathbf{H}\cdot\mathbf{I} + \mathbf{S}\cdot\mathbf{A}_N\cdot\mathbf{I} + \hbar\mathbf{I}\cdot\mathbf{Q}\cdot\mathbf{I} \quad (1)$$

Here, g_N and β_N are the nuclear g factor and Bohr magneton, **H** is the external magnetic field, and **I** is the nuclear spin operator; $\mathbf{A}_N$ is the superhyperfine tensor and **S** is the electron spin operator; $\hbar$ is Planck's constant and **Q** is the quadrupole interaction tensor.

In a $d_{x^2-y^2}$ ground-state Cu(II) complex, when ^{14}N on an equatorial metal ligand is directly coordinated to the metal ion, the electron–nuclear interaction is large and dominates the electromagnetic coupling. This coupling is outside the range applicable for ESEEM methods,[30,31] and one can resort to conventional, CW EPR or to ENDOR spectroscopy for its study. On the other hand, when ^{14}N on an equatorial metal ligand is not directly coordinated to Cu(II) or when it is directly coordinated to Cu(II) axially, the electron–nuclear hyperfine interaction is considerably weaker and may be comparable in magnitude to the nuclear Zeeman interaction. Under these conditions, the magnetic coupling becomes dominated by the nuclear quadrupole interaction and ESEEM spectroscopy is particularly well-suited for the investigation of such systems.[20,30,32]

When the electron–nuclear hyperfine coupling and the nuclear Zeeman interaction for a ^{14}N nucleus on a Cu(II) ligand are nearly equivalent, deep modulations are observed in the electron spin echo decay envelope.[30] Subsequent to Fourier transformation, a typical ^{14}N ESEEM spectrum is obtained having three intense, sharp lines and one relatively weaker, broad line at a higher frequency. The three sharp low-frequency lines arise from the spin manifold where the electron–nuclear hyperfine interaction is canceled by the nuclear Zeeman interaction and the nuclear quadrupole interaction solely determines their energy differences.[30,32] Their frequencies are, therefore, almost field independent and comparable to the NQR frequencies, ν_0 and $\nu_\pm$, given by eqs 2 and 3 for non-paramagnetic complexes.

$$\nu_\pm = {}^3/_4 e^2qQ(1 \pm \eta/3) \quad (2)$$

$$\nu_0 = {}^1/_2 e^2qQ\eta \quad (3)$$

Here, the quadrupole coupling constant e^2qQ and the asymmetry parameter η measure the magnitude and the symmetry of the quadrupole tensor **Q** and the electric field gradient tensor **q**, where $\mathbf{Q} = e^2\mathbf{q}Q$ and Q is the quadrupole moment of ^{14}N. The sum of the frequencies of the first two lines in the ESEEM spectrum is equal to that of the third. The intensities of these lines are mainly determined by the orientation of the efg tensor relative to the **g** tensor, described by the Euler angles, α, β, and γ.[20]

The broader, high-frequency line arises from the other spin manifold where the electron–nuclear hyperfine interaction is doubled by the Zeeman interaction. Because of the anisotropy of the electron–nuclear hyperfine coupling, the transition frequency of this manifold varies for molecules with different molecular orientations, so that for a frozen solution sample the frequency observed is an average of contributions from all of those excited at a particular magnetic field setting. As a result, single-quantum transitions (ΔM_I = 1) cannot be observed due to this averaging effect.[33] The double-quantum transition (ΔM_I = 2) is observed as a broad line at approximately $2g_N\beta_N H + a$, where a is the electron–nuclear coupling. The frequency of this line depends mainly on the magnetic field and the electron–nuclear coupling, and its shape and intensity depend on the polar and azimuthal angles, θ_N and ϕ_N,[34] and the Euler angles described earlier. Field-dependent ESEEM spectral simulations across the EPR absorption can be used to determine these superhyperfine parameters.[20]

The ESEEM spectrum of [Cu(II)(TEPA)($^{14}NO_2$)]PF_6 obtained at a τ value 3 times the proton periodicity[35,36] is shown in

(27) (a) Cotton, F. A.; Wilkinson, G. *Advanced Inorganic Chemistry*, 5th ed.; Wiley-Interscience: New York, 1988; p 486. (b) Nakamoto, K. *Infrared and Raman Spectra of Inorganic and Coordination Compounds*, 4th ed.; Wiley-Interscience: New York, 1986; pp 221–227.

(28) Tolman, W. B. *Inorg. Chem.* **1991**, *30*, 4877–4880.

(29) $A_\perp$ cannot be accurately determined. The value is estimated directly from the splitting at $g_\perp$ region of the spectrum and has no effect on later ESEEM simulations.

(30) Mims, W. B.; Peisach, J. *J. Chem. Phys.* **1978**, *69*, 4921–4930.

(31) Mims, W. B.; Peisach, J.; Davis, J. L. *J. Chem. Phys.* **1977**, *66*, 5536–5550.

(32) Jiang, F.; McCracken, J.; Peisach, J. *J. Am. Chem. Soc.* **1990**, *112*, 9035–9045.

(33) Colaneri, M. J.; Potenza, J. A.; Schugar, H. J.; Peisach, J. *J. Am. Chem. Soc.* **1990**, *112*, 9451–9458.

(34) The electron–nuclear hyperfine coupling is taken to be axial, with a point dipole–dipole approximation. Its magnitude is described by A_{iso}, the isotropic component of the coupling, and r_{eff}, the effective distance between the unpaired electron and the interacting nucleus. Due to the axial nature of the coupling tensor, two angles θ_N and ϕ_N, which specify the apparent spherical polar coordinates of the interacting nucleus, are sufficient to describe the orientation of the principal axis of this tensor relative to that of the **g** tensor.

(35) ESEEM spectra of 1 prepared with $^{14}NO_2^-$ and $^{15}NO_2^-$, and obtained at a τ value twice the proton periodicity were shown to be dominated by contributions from the directly coordinated axial pyridyl nitrogen. These were identified from their presence in the ESEEM spectra of [Cu(II)(TEPA)(Cl)]PF_6 and of [Cu(II)(TEPA)(NO_3)]NO_3 (data not shown). Since our interest is in the nitrite nitrogen, the characterization of the axial pyridyl nitrogen has not been pursued.

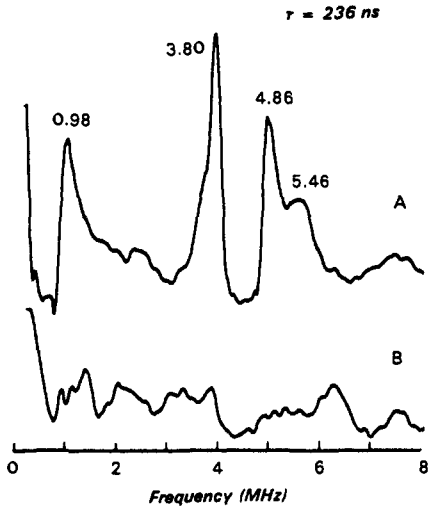

Figure 4. ESEEM spectra of **1** prepared with (A) $^{14}NO_2^-$ and (B) $^{15}NO_2^-$ studied at a τ value of 3 times the proton periodicity. Experimental conditions: microwave frequency, 8.55 GHz; magnetic field, 2981 G; τ = 236 ns. The modulations from the axial pyridine ^{14}N are much weaker than those from $^{14}NO_2^-$ so that modulations from the former can be ignored and the sharp lines can be assigned to the nitrite ^{14}N.

Figure 4A. Two nitrogen populations give rise to modulations, the directly coordinated axial pyridyl nitrogen and the non-directly coordinated equatorial nitrite nitrogen. The other directly coordinated nitrogen atoms are coupled too strongly to give modulations.[30,32] On the basis of a comparison with the spectrum obtained for the complex prepared with $^{15}NO_2$ (Figure 4B), one notes that the combined spectral contributions from the axial pyridyl ^{14}N and the equatorial nitrite ^{15}N have an amplitude of about 20% of those in Figure 4A. We assign the lines in Figure 4A to the equatorially coordinated $^{14}NO_2$ and ignore the lesser contributions from the pyridyl ^{14}N in subsequent analysis.

Nitrogen Modulations from $^{14}NO_2^-$. ESEEM spectra obtained at six different magnetic field settings with a τ value 3 times the proton periodicity are shown in Figure 5A. In the spectra collected at the middle of the EPR absorption, where an average of many molecular orientations occurs, one observes three intense, narrow lines at about 1.0, 3.8, and 4.9 MHz. The frequencies of the lower two lines approximately add to give the third, and they remain virtually unchanged at almost all the magnetic field settings studied, except the one nearest the low-field end of the EPR absorption. This is characteristic of NQI lines where the nuclear Zeeman interaction for ^{14}N is comparable to the electron–nuclear coupling. A broader and weaker line, above 5.5 MHz, changes in frequency when the external magnetic field setting is altered. This is characteristic of the field dependence of the $\Delta M_I = 2$ transition for ^{14}N. On the basis of this line assignment, the quadrupole and electron–nuclear coupling constants can be obtained from simulations of the spectral frequencies.[14,18,32]

Spectra obtained near the low-field end of the CW EPR absorption, e.g. at 2620 and 2520 G, however, do not have well-characterized features. A new broad feature around 1.5 MHz appears. Especially at 2520 G, the 1-MHz line disappears, and instead, two broad lines at about 1.4 and 1.7 MHz dominate the spectrum. At 2520 G, only very few orientations are excited due to the anisotropy of the **g** tensor. The dramatic change of the spectrum from those obtained at higher fields suggests that the electron–nuclear coupling is highly anisotropic. Due to this anisotropy, we are able to obtain not only the coupling constants but also the orientation parameters by angle-selective ESEEM simulations.[20]

Hyperfine Coupling Constants. Assuming that r_{eff} is 2.75 Å, the distance between Cu(II) and the nitrite nitrogen as determined by X-ray crystallography, values for e^2qQ of 5.66 MHz, η of 0.31, and A_{iso} of 3.05 MHz were first obtained in a spectral simulation at 2740 G. The fit is good for the NQI lines whose frequencies are sensitive to e^2qQ and η. Because e^2qQ is large, a small change of η results in a significant change in the frequencies of the NQI lines (eqs 2 and 3). The error in determining η is 0.02, a value much less than that for amino nitrogen, 0.5, where e^2qQ is considerably smaller.[32]

The fit to the double-quantum line in the spectrum at 2740 G (and at other fields as well) was not as good. In the experimental data, a split double-quantum line is seen, with features at 5.8 and 6.6 MHz (Figure 5A). A line at 6.6 MHz with a higher frequency shoulder was obtained in the simulation. Also, the double-quantum features did not shift with magnetic field as much as was observed in the experimental data, suggesting a need for greater anisotropy in the simulation. Therefore, even though the NQI parameters used are appropriate to give a good fit for the three lower frequency sharp lines of the spectrum, the electron–nuclear hyperfine constants used in the simulation may not best describe the system.

As shown in Figure 5A, the frequency of the $\Delta M_I = 2$ line decreases slightly when the magnetic field increases from 2520 G; it splits into two lines at 2740 G, achieves a minimum value at 2981 G (near $g_\perp$), and then increases again at 3082 G. A smaller value for r_{eff} to achieve larger anisotropy was needed to properly simulate the spectra. Reducing r_{eff} to 2.0 Å and increasing A_{iso} to 3.40 MHz gave the split double-quantum features observed at 2740 G with correct frequencies, as well as good fits for the double-quantum features across the EPR absorption.[38]

The value of r_{eff} used in a spectral simulation is taken as the distance between the unpaired electron spin and the ^{14}N nucleus assuming a point-dipole dipole interaction. Because the unpaired electron delocalizes onto the ligand, there is some unpaired electron spin density at the coordinated oxygen. This gives rise to an isotropic component, A_{iso}, for the electron–nuclear coupling, due to the spin polarization at the ^{14}N. Therefore, r_{eff} is expected to be shorter than the actual distance between the Cu(II) and ^{14}N. In our simulations, the best fit was achieved with r_{eff} 27% shorter than the actual distance. This phenomenon has been demonstrated for other systems studied by ESEEM as well. The anisotropic coupling between the unpaired electron of Cu(II) and the remote ^{14}N of coordinated imidazole in copper(II)–dien–imidazole is best described by an r_{eff} of 3.20 Å, 22% shorter than the actual distance between the Cu(II) and the ^{14}N examined.[32] Also, in the case of copper(II)–[^{2}H]glycine, the deuterium modulations obtained were more intense than expected from the known Cu(II)–^{2}H distance.[31]

Orientation of Hyperfine Tensors. The direction of the principal axis of the **g** tensor is closely related to the symmetry of the Cu(II) site. For a square pyramidal complex, the *xy* plane of the **g** tensor is in the plane of the square encompassing the four close equatorial ligands to the metal ion, and the g_z axis points in the direction of the axial ligand. As shown from the X-ray diffraction of **1**, the amine nitrogen, two pyridyl nitrogens, and a nitrite oxygen form an approximate plane, and the axial Cu(II)–N_4 bond is approximately perpendicular to this plane (Figure 1). If the same

(36) An attempt was made to ratio the modulation data of [Cu(II)(TEPA)($^{14}NO_2$)]PF_6 with that of [Cu(II)(TEPA)($^{15}NO_2$)]PF_6 obtained at a τ value 2 times the proton periodicity in order to eliminate the contributions from the axial pyridyl nitrogen and to reveal those from the equatorial $^{14}NO_2$.[37] This was followed by Fourier transformation of the resulting quotient, subsequent to dead-time reconstruction. Because the modulations from both the axial and equatorial nitrogen are very weak and have similar amplitudes, the ratioed data were extremely noisy and we could not better resolve the features from bound $^{14}NO_2$ in the Fourier transform.

(37) Zweier, J.; Aisen, P.; Peisach, J.; Mims, W. B. *J. Biol. Chem.* **1979**, *54*, 3512–3518.

(38) On the basis of a value of 3.40 MHz for the nitrite ^{14}N, one would predict an A_{iso} value of 4.77 MHz for the ^{15}N analog, correcting for the relative gyromagnetic ratio of the two isotopes. We would expect a two-line spectrum, approximately centered at $A_{iso}/2$ and offset by ±1.2 MHz, the ^{14}N nuclear Zeeman frequency at the magnetic field employed, near 1.2 and 3.6 MHz. A broad feature can be observed at 1.2 MHz in the spectrum of [Cu(II)(TEPA)($^{15}NO_2$)]PF_6 (Figure 4B), not observed for [Cu(II)(TEPA)($^{14}NO_2$)]PF_6. The contributions from the axial pyridine ^{14}N, a line near 3.8 MHz, does not allow us to resolve any putative ^{15}N contribution in that region of the spectrum. Further, the large anisotropy obtained for the $^{14}NO_2$ complex may complicate this analysis.

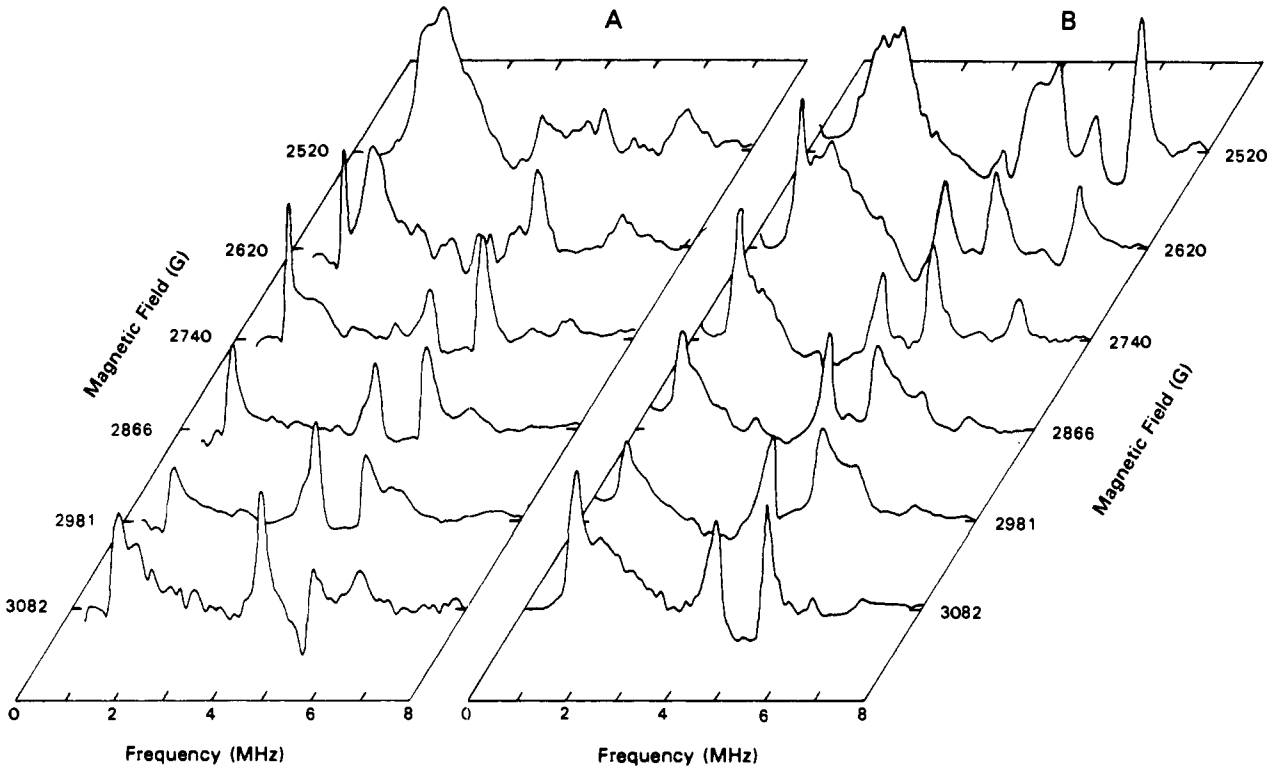

Figure 5. Three-pulse ESEEM spectra (A) and spectral simulation (B) of $[Cu(II)(TEPA)(^{14}NO_2)]PF_6$ at six different magnetic field settings within the EPR absorption. Echo envelope modulations were collected at a microwave frequency of 8.55 GHz at the magnetic fields indicated. Three intense, narrow lines appearing in most of the spectra are assigned as the NQI transitions, while the high-frequency line above 5 MHz is assigned as the $\Delta M_I = 2$ transition.

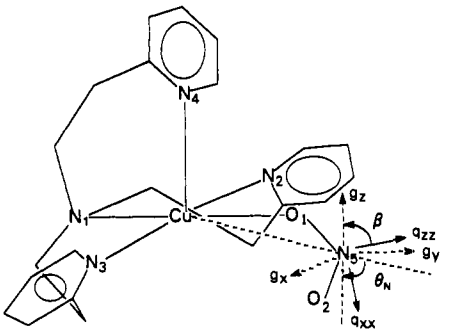

Figure 6. Schematic drawing of **1** and the axis system of the **g** tensor and of the electric field gradient tensor (**q**) at the nitrite ^{14}N. The principal direction q_{zz} is at the lone-pair sp^2 orbital, along the bisector of ∠O(1)N(5)O(2) and in the nitrite plane; q_{yy} is perpendicular to the nitrite plane (not shown). The directions of g_x and g_y are placed arbitrarily in the equatorial plane.[38]

structure of **1** is retained in frozen solution, we may first assume that the g_z axis is along the N(4)–Cu(II) bond. The polar angle θ_N for the ^{14}N studied (Figure 6) would be the supplementary angle of N(4)–Cu(II)–N(5), which is about 60°. Because g_x and g_y can be along any direction in the equatorial plane,[39] the azimuthal angle ϕ_N is assumed to be 0°.

For the nitrite ^{14}N, the direction of the principal axis of the quadrupole tensor is determined by the direction of the valence shell orbitals. The nitrogen atom is an approximate sp^2 hybrid, with two sp^2 orbitals involved in the N–O σ bonds and the third having a lone pair of electrons. The p orbital, perpendicular to the sp^2 orbitals (O–N–O plane), is involved in π bonding with oxygens. In crystalline sodium nitrite,[40,41] the two N–O bonds are equivalent so that the lone-pair orbital, in which excess electrons generate the largest electric field gradient, is along the bisector of the ONO angle. The direction with the largest principal value, q_{zz}, is thus along the bisector of the ONO angle; q_{xx} is in the O–N–O plane and perpendicular to the lone-pair orbital, and q_{yy} is perpendicular to the O–N–O plane, along the p orbital.[40,41] For **1**, although the binding of NO_2^- to the Cu(II) through one of the oxygen atoms leads to slight inequivalence of the N–O bonds, it is still reasonable, to a good approximation, to assume that the principal axis of the quadrupole tensor is the same as that in sodium nitrite (Figure 6).[42] Further, if we assume that the structure of **1** in frozen solution is the same as that in the crystal, the Euler angles between the principal axis of the quadrupole tensor and the **g** tensor can be determined. The angle needed to rotate q_{zz} into g_z, β, would be about 75°, the angle between the bisector of O–N–O and N(4)–Cu(II). The angle γ, like ϕ_N, is assumed to be 0°.

With 60°, 0°, and 0° obtained from the crystal structure as starting values for θ_N, ϕ_N, and γ in an ESEEM spectral simulations, α and β were individually varied in 10-deg increments to fit the spectrum collected at 2740 G. The frequency of the NQI lines are affected only slightly by the change of angles so that the determination of e^2qQ and η is virtually independent of the angles used. However, the relative intensities of the NQI lines were found

(39) The crystal structure shows that the two almost equivalent equatorial pyridyl nitrogens and the Cu(II) lie in a straight line, which defines a geometric direction, while the amine nitrogen and nitrite oxygen lie in a line directed perpendicular to the former. Because of the structural inequivalency in these two directions, the values of g_x and g_y would be expected to differ slightly from one another and to lie along the above two directions. Since the inequivalency of g_x and g_y cannot be resolved in the frozen solution CW EPR spectrum, we assume them to be equal. In other words, it is reasonable to assume the g_x and g_y axes along any direction in the xy plane.

(40) Ikeda, R.; Mikami, M.; Nakamura, D.; Kubo, M. *J. Magn. Reson.* **1969**, *1*, 211–220.

(41) Marino, R. A.; Bray, P. J. *J. Chem. Phys.* **1968**, *48*, 4833–4838.

(42) A microwave study of *trans*-HNO_2[43] shows that q_{zz} is only 4° off the bisector of ∠ONO, even though the two N–O bond lengths differ by 0.256 Å, with q_{yy} perpendicular to the ONO plane. Since the two N–O bonds in our model differ by only 0.06 Å, the deviation of q_{zz} from the bisector of ONO must be less than 4°, which is well within the error of our experiment. Therefore, our assumption for the principal directions of the quadrupole tensor is reasonable.

(43) Cox, A. P.; Kuczkowski, R. L. *J. Am. Chem. Soc.* **1966**, *88*, 5071–5075.

Table IV. Superhyperfine Parameters for $^{14}NO_2^-$ in Compound **1**

nuclear quadrupole interaction	electron–nuclear coupling
e^2qQ = 5.66 MHz	A_{iso} = 3.40 MHz
η = 0.31	r_{eff} = 2.0 Å
α = 20°	θ_N = 50°
β = 90°	ϕ_N = 0°
γ = 0°	

to be most sensitive to β, so that as it is increased from 0° to 90°, the intensity of the 1-MHz line increases dramatically. At a β value of 90°, this line dominates the spectrum and all the others are less than $^1/_4$ as strong. The change of α from 0° to 90° has an opposite effect as that from changing β. Simulations with a small value for α and a large value for β or a large value for α and a small value for β give the correct relative NQI line intensities.

The spectrum obtained at the lowest magnetic field setting (2520 G), which is most single-crystal like and most sensitive to the Euler angles, was simulated to refine α and β. Four coupling constants, as well as θ_N, ϕ_N, and γ, were adjusted. With a large value for α and a small value for β, we obtained the unusual features at 1.4 and 1.8 MHz seen in the experimental data. But simulations at higher field settings did not fit as well. With a small value for α and a large value for β, θ_N had to be decreased by 10° to obtain the features at 1.4 and 1.8 MHz. The best fit for all six spectra was achieved with θ_N and ϕ_N of 50° and 0°, and α, β, and γ of 20°, 90°, and 0°, as shown in Figure 5B (the simulation parameters are summarized in Table IV).[44] A change of 10° in either θ_N, α, or β resulted in a dramatic change of the quality of the fit, while alterations of 10° in ϕ_N or γ had less effect.

The values for θ_N and β of 50° and 90° obtained from the spectral simulations are slightly different from the values of 60° and 75° calculated from the crystal structure and the assumed **g** tensor principal axis. This slight inconsistency can be attributed to the approximation made for the principal directions of the **g** tensor. X-ray diffraction and single-crystal EPR studies of $[Cu(terpy)(NO_2)OH_2]^+$, a square planar complex structurally analogous to $[Cu(II)(TEPA)(NO_2)]^+$, showed that the *xy* plane of the **g** tensor is defined by three strongly coupled, equatorially coordinated nitrogens and g_z is perpendicular to this plane, 6° away from the axial Cu–O(H_2) direction.[23] For **1**, the direction perpendicular to the plane defined by the three equatorially coordinated nitrogens is about 9° tilted away from the Cu–N(4) direction toward Cu–N(1). By analogy, this should be the direction of g_z. As a result, θ_N should be reduced by 9° to 51° and β increased by 9° to 84°, consistent with the simulation results (Figure 6, Table IV). This agreement between the simulation results and the values obtained from the crystal structure suggests that in frozen solution the nitrite ONO orientation relative to the Cu(II)(TEPA) structure is the same as that found in the crystal.[45]

Nuclear Quadrupole Parameters and Electron Distribution. The nuclear quadrupole parameters for NO_2^- in a variety of diamagnetic solids with either monovalent cations[41,46,47] ($NaNO_2$, KNO_2, $LiNO_2{\cdot}H_2O$, $CsNO_2$) or divalent cations[46] ($Ca(NO_2)_2{\cdot}H_2O$, $Sr(NO_2)_2{\cdot}H_2O$, $Ba(NO_2)_2{\cdot}H_2O$) have been obtained by nuclear quadrupole resonance spectroscopy. The magnitude of e^2qQ for the various nitrite compounds enumerated above ranges within 1.7% of an average value of 5.62 MHz, depending on the cation of the complex. The variation of η is about 5% with an average value of 0.367. Although an η value of 0.31 obtained for NO_2^- in **1** is slightly smaller than the average value obtained by NQR studies (this will be discussed later), the value of 5.66 MHz for e^2qQ from our study falls in the range from NQR investigations, supporting our spectral assignment for NO_2^- modulations and our spectral simulations.

The unusually large value of e^2qQ for NO_2^-, as compared to other nitrogen-containing compounds, arises from the presence of two whole electrons in the nonbonding lone pair sp^2 orbitals of ^{14}N and a deficiency of electrons in the other two sp^2 orbitals (the bonding oxygen has a higher electronegativity). For $NaNO_2$, the crystal structure[48] shows that the Na^+ is close to the oxygen and separated from the nitrogen by a distance of 2.4 Å along the bisector of the ONO angle. The nitrogen lone-pair orbital has two electrons and is not involved in binding to other nuclei in its vicinity. Were the nitrogen lone-pair orbital perturbed, such as by coordination to a metal ion, a decrease of the electron population would occur and a decrease of e^2qQ would be expected.[49] Therefore, the large e^2qQ value obtained for Cu(II)(TEPA)-coordinated nitrite in frozen solution is in accord with NO_2^- binding to Cu(II) through oxygen, rather than through nitrogen, consistent with the IR and the X-ray diffraction results.

Net Charge on Nitrite Nitrogen and the ONO Angle. The net charge on a ^{14}N nucleus is determined by the electron distribution at this nucleus, whose assessment would require a precise knowledge of the molecular wave function of the complex. To a first-order approximation, we can use the Townes and Dailey theory[6] to obtain the electron population in the bonding orbital of NO_2^- from the quadrupole parameters. According to this theory, only p electrons in the valence shell contribute to the electric field gradient; inner closed or s shells are spherically symmetric and the electrons of other atoms contribute negligibly since the electric field gradient has a $\langle 1/r^3 \rangle$ dependence.

If we assume that the two N–O sp^2 orbitals of NO_2^- have an approximately equal electron population of σ_{no},[51] the lone pair sp^2 orbital has a population l, and the pπ orbital has a population π, then the electric field gradient generated along the three principal axes is given by eqs 4–6.

$$q_{zz} = q_0[(1 - \cot^2\theta)l - \tfrac{1}{2}\pi + (\cot^2\theta - \tfrac{1}{2})\sigma_{NO}] \quad (4)$$

$$q_{yy} = q_0[-\tfrac{1}{2}(1 - \cot^2\theta)l - \tfrac{1}{2}\pi + (1 - \tfrac{1}{2}\cot^2\theta)\sigma_{NO}] \quad (5)$$

$$q_{xx} = q_0[-\tfrac{1}{2}(1 - \cot^2\theta)l + \pi - \tfrac{1}{2}(1 + \cot^2\theta)\sigma_{NO}] \quad (6)$$

Here, 2θ is the $\angle$ONO, e^2q_0Q is the electron field gradient arising

(44) The field width ΔH was varied in spectral simulations in order to evaluate its effect on the determination of tensor orientations. When ΔH was increased from 20 to 50 G, only the relative intensities of lines in the simulated spectra obtained at intermediate field settings were affected, but not their frequency positions. Here many orientations are selected due to the *g* and metal hyperfine anisotropy. However, at the high-field end of the EPR absorption (3082 G), no orientations were found to be on resonance using a ΔH of 20 G, suggesting that a larger field width should be used to select more orientations. A simulated spectrum was obtained using a ΔH of at least 30 G. On the other hand, at the low-field end of the EPR absorption (2640 G), using ΔH of 20 G in a spectral simulation, the data were well duplicated. When ΔH was increased from 20 to 50 G, a ~1 MHz line was obtained in the simulated spectrum. This was not seen in the experimental spectrum at this field but is observed at higher magnetic field settings when more orientations are selected. With a reduction of θ by 5° (from 50° to 45°), the 1-MHz line is lost in the simulation. However, changing the value of θ affected the frequencies in simulated spectra at higher field settings so that they did not match the experimental data as well, even after adjusting other parameters. Therefore, a θ value of 50° better represents the data while too many orientations were selected using ΔH of 50 G. An intermediate ΔH, 40 G, was then used in the simulations.

(45) The O(1)N(5)O(2) plane is not perpendicular to the N(1)N(2)N(3) plane, indicating that a rotation along q_{zz} is needed to bring q_{yy} into the *xy* plane of the **g** tensor. The simulation result for α leads us to conclude that this angle is 20°.

(46) (a) Oja, T.; Marino, R. A.; Bray, P. J. *Phys. Lett.* **1967**, *26A*, 11–12. (b) Marino, R. A.; Oja, T.; Bray, P. J. *Phys. Lett.* **1968**, *27A*, 263–264.

(47) Matushin, O. L.; Saf, D. Y. *Proc. Russian Acad. Sci.* (*E* and **3**) **1975**, *39*, 2472.

(48) (a) Carpenter, G. B. *Acta Crystallogr.* **1952**, *5*, 132–135. (b) Truter, M. R. *Acta Crystallogr.* **1954**, *7*, 73–77. (c) Ziegler, A. E. *Phys. Rev.* **1931**, *38*, 1040–1047.

(49) This has been shown for other sp^2 hybrid nitrogens. The value of e^2qQ drops from 5.0 to 3.4 MHz[50a] when glyoxime binds to Pd through the nitrogen lone pair orbital. Also, the value of e^2qQ for carbon–nitro compounds drops to 1.5 MHz[50b] when the electron population of the "lone-pair" orbital decreases to about 1 by forming a covalent bond with carbon.

(50) (a) Hsieh, Y.-N.; Ireland, P. S.; Brown, T. L. *J. Magn. Reson.* **1976**, *21*, 445–456. (b) Subbarao, S. N.; Sauer, E. G.; Bray, P. J. *Phys. Lett.* **1973**, *42A*, 461–462.

(51) The electron populations σ_{NO} of the two N–O sp^2 orbitals of NO_2^- are equal, since the two N–O bonds are equivalent. The binding of nitrite to Cu(II)(TEPA) through one of the oxygens makes the N–O bonds slightly inequivalent (0.06 Å). In this case, σ_{NO} should be the average of the electron populations of the two N–O sp^2 orbitals. Equations 4–6 remain valid.

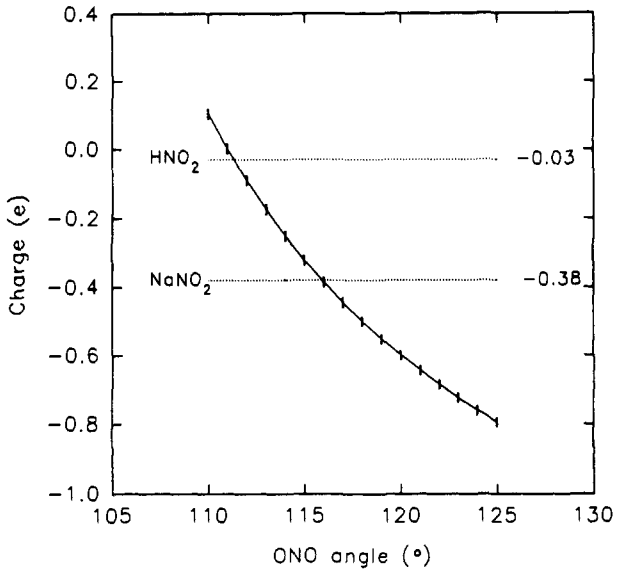

Figure 7. Plot of the net charge on nitrite nitrogen vs ONO angle, with ^{14}N having quadrupole parameters e^2qQ = 5.66 MHz and η = 0.31. The ONO angle giving the net charge on nitrogen between that of HNO_2 and $NaNO_2$ is limited to be within 112° and 116°.

from an unbalanced p electron,[52] and $|q_{zz}| > |q_{yy}| > |q_{xx}|$.[54] The quadrupole parameters are determined by eqs 7 and 8.

$$e^2qQ = e^2q_0Q[(1 - \cot^2\theta)l - \tfrac{1}{2}\pi + (\cot^2\theta - \tfrac{1}{2})\sigma_{NO}] \quad (7)$$

$$e^2qQ\eta = e^2q_0Q[\tfrac{3}{2}(\sigma_{NO} - \pi)] \quad (8)$$

Assuming l is 2, the electron population for the lone-pair electrons, π and σ_{NO}, can then be obtained from e^2qQ and η, when θ is known. The charge on the nitrogen atom, ρ_N, can be obtained from eq 9.

$$\rho_N = 3 - 2\sigma_{NO} - \pi \quad (9)$$

This was calculated for NO_2^- in solid $NaNO_2$, where e^2qQ is 5.79 MHz, η is 0.405, and ∠ONO is 115°.[40] The value for σ_{NO} was calculated as 1.18 and that for π as 1.02, which gives a net charge of −0.38 e on the nitrogen and −0.31 e on each of the oxygen atoms. The net charges obtained this way are in good agreement with the corresponding values of −0.36 and −0.32 e estimated from spontaneous polarization studies.[56]

The net charge on the nitrite nitrogen in **1** can be calculated for a given ONO angle, using the quadrupole parameters obtained by ESEEM spectral simulation. In previous studies of various crystalline Cu(II)−NO_2^- complexes,[24-26,28] the ONO angle for NO_2^- was shown to vary from 110° to 125°. Figure 7 shows the net charge at the nitrite nitrogen calculated for this range of angles. The charges obtained the same way for solid $NaNO_2$ and gaseous *trans*-HNO_2 are −0.38 and −0.03 e, respectively. They can be considered as the lower and upper limits for the charge on the nitrite nitrogen in **1**, considering the total negative charge on NO_2^-. In **1**, one of the nitrite oxygens donates a lone-pair electron to Cu(II) to form a coordinate covalent bond; hence, the total negative charge on NO_2^- is expected to be less than that of solid $NaNO_2$, where NO_2^- bears a full negative charge. Furthermore, it is expected to be greater than that of gaseous *trans*-HNO_2, where NO_2 donates almost a whole electron to form a covalent bond with H. The ONO angle of nitrite is, therefore, limited between 111.4° and 116.0°, on the basis of the quadrupole parameters we obtained by ESEEM for frozen solutions of **1**. This value compares well with 114.9° found in the crystal by X-ray diffraction.

Factors that Affect η. The value of η obtained for the nitrite ^{14}N in **1** is smaller than that in solid, ionic metal nitrite complexes. This may arise from the difference of charge distribution in frozen solution from that in solids. Marino and Bray[41] have estimated that, in solid $NaNO_2$, one quarter of η is due to the presence of lattice charges, although this only produces small errors in electron populations.

The smaller value for η may also arise from the inequivalency of the two N–O bonds when nitrite binds to Cu(II)(TEPA) mainly through one of the oxygen atoms. A microwave spectroscopic study[43] shows that ^{14}N in gaseous *trans*-HNO_2 has an even smaller value for η, 0.29. It also shows that the N—O(H) bond and the N═O bond differ in length by 0.256 Å, as compared to 0.06 Å for the two N–O bonds of **1**. Although a 5% change is expected for e^2qQ when HNO_2 changes from the gaseous state to the solid state due to the internal field and lattice vibration, η is unaffected.[57] For sodium nitrite, where the two N–O bonds have essentially the same bond length, η is 0.405. It is reasonable that the inequivalency of the two N–O bonds of the nitrite in our model complex results in a reduction in the η value from that found in solid sodium nitrite, but in an increase from that found in gaseous HNO_2.

EPR and ESEEM of the Nitrite Derivative of Hemocyanin. Hemocyanin contains a dicuprous center capable of reversible dioxygen binding. The protein can also be oxidized to the met or dicupric form as well as to various half-met forms where one of the copper atoms is cuprous and the other cupric.[4b] One of the earliest studied reactions of hemocyanin is that with NO.[58] The EPR-active product of the reaction is believed to be the same as that formed with nitrite, either in the presence or absence of ascorbate. As the observed EPR signal intensity accounts for only half the protein-bound copper, it was suggested that the product of the NO reaction was a half-met derivative, with NO bound to EPR-active copper. However, Van der Deen and Howing[59] failed to observe any difference in the EPR properties of the derivative formed in a reaction with either [^{14}N]- or [^{15}N]nitrite, and an infrared investigation could not substantiate that NO was bound at all. In a subsequent study, Verplaeste et al.[60] did find a single equivalent of NO bound per equivalent of EPR-detectable copper by chemical analysis and suggested that the NO was coordinated to the EPR-silent Cu(I) at the binuclear center of a half-met form of the protein. As the NO was not coordinated to Cu(II), no difference in EPR was expected.

A totally different interpretation was afforded by Solomon,[4b] Himmelwright et al.,[4a] and Westmoreland et al.,[61] who argued that nitrite, when reacted with hemocyanin, becomes a tightly bound, bridging ligand between Cu(I) and Cu(II), with Cu(II) bound to the nitrite oxygen atom. It is understandable with the proposed formulation that no difference in EPR spectra was expected for a derivative made with either [^{14}N]- or [^{15}N]nitrite,

(52) The term e^2q_0Q is the nuclear quadrupole coupling constant for an ^{14}N atom with an unbalanced p electron. Depending on the total charge on the atom in question, the coupling constant varies. This value has been chosen between 8 and 10 MHz[40,53] in NQR studies to reach an agreement with theoretical calculations. To be consistent with early works on NO_2^-,[40,41] the value of 10 MHz is used in the present investigation.

(53) (a) Guibe, L.; Lucken, E. A. C. *Mol. Phys.* **1966**, *10*, 273–281. (b) Shempp, E.; Bray, P. J. *J. Chem. Phys.* **1967**, *46*, 1186–1190.

(54) Several LCAO-SCF-MO calculations[55] for NO_2^- have shown that $\pi < \sigma_{NO}$. Since $q_{11} - q_{\perp\perp} = \frac{3}{2}(\sigma_{NO} - \pi) > 0$, with our assignment of the principal axis, we have $|q_{zz}| > |q_{11}| > |q_{\perp\perp}|$. The quadrupole coupling constants for *trans*-HNO_2 from a microwave study[43] are in fair agreement with those we obtained for our model complex, indicating that NO_2^- and HNO_2 resemble each other, at least regarding the electronic structure about their respective nitrogen nuclei. The principal axes of the quadrupole coupling tensor of HNO_2, which are almost coincidental with the symmetry axis of the molecule, are in accord with our assignment.

(55) (a) Petrongolo, C.; Scrocco, E.; Tomasi, J. *J. Chem. Phys.* **1968**, *48*, 407–411. (b) Bonaccorsi, R.; Petrongolo, C.; Scrocco, E.; Tomasi, J. *J. Chem. Phys.* **1968**, *48*, 1497–1499.

(56) Kay, M. I.; Frazer, B. C. *Acta Crystallogr.* **1961**, *14*, 56–57.

(57) Lucken, E. A. C. *Nuclear Quadrupole Coupling Constants*; Academic: New York, 1969; pp 147–155.

(58) Phillips, S. E. V.; Stevens, C.; Ogel, Z. B.; McPherson, M. J.; Keen, J. N.; Schoot Uiterkamp, A. J. M. *FEBS Lett.* **1972**, *20*, 93–96.

(59) Van der Deen, H.; Howing, H. *Biochemistry* **1977**, *16*, 3519–3525.

(60) Verplaetse, J.; Van Tornout, P.; Defreyn, G.; Witters, R.; Lontie, R. *Eur. J. Biochem.* **1979**, *95*, 327–331.

(61) Westmoreland, T. D.; Wilcox, D. E.; Baldwin, M. J.; Mims, W. B.; Solomon, E. I. *J. Am. Chem. Soc.* **1989**, *111*, 6106–6123.

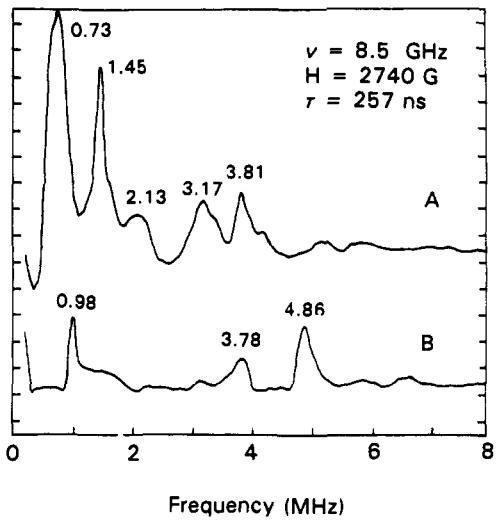

Figure 8. Three-pulse ESEEM spectra of (A) the $^{14}NO_2^-$ derivatives of hemocyanin and (B) [Cu(II)(TEPA)($^{14}NO_2$)] studied under similar experimental conditions. Measurement conditions: microwave frequency, (A) 8.50 GHz and (B) 8.55 GHz; magnetic field, 2740 G; τ = 257 ns. The lines observed in spectrum A are attributed to multiple remote nitrogens of Cu(II)-coordinated histidine imidazoles.

as the electron–nuclear coupling to nitrogen would undoubtedly be too weak to resolve with conventional EPR.

The arguments supporting nitrite as a bridging ligand are not direct and rely heavily on an analysis of spectroscopic data.[61] An independent argument for nitrite as a bridging ligand between both copper atoms at the active site is based on the sluggishness of reactivity of the nitrite derivative with azide, as compared to the same reaction for the half-met aquo derivative of the protein. Yet chemical analysis of the hemocyanin product of the nitrite reaction[5] showed that the amount of bound nitrite was far less than stoichiometric with the EPR detectable copper, especially for preparations produced under anaerobic conditions.

Since the arguments for bridging nitrite coordination are largely inferential rather than direct, it was felt that a specific test should be made for its presence by probing for weak ^{14}N magnetic coupling arising from a putative exogenous nitrogenous ligand to Cu(II) using ESEEM spectroscopy. The ESEEM spectrum for the $^{14}NO_2^-$ derivative of hemocyanin is shown in Figure 8A. An identical spectrum is obtained for the preparation made with $^{15}NO_2^-$ (not shown), and both are significantly different from those obtained for [Cu(II)(TEPA)($^{14}NO_2$)]PF_6 (Figure 8B). For the protein, one broad and one narrow line are obtained in the low-frequency region of the spectrum at 0.73 and 1.45 MHz, with the broader one consisting of two unresolved lines. These are characteristic ^{14}N modulations arising from the remote nitrogen of Cu(II)-coordinated histidine imidazole.[30,32] The presence of a sum frequency of 2.13 MHz (the sum of 0.73 and 1.45 MHz) is indicative of multiple imidazole coordination to Cu(II).[62] This is consistent with the X-ray crystal structure of deoxy hemocyanin, where each of the copper atoms is bound to two close-lying imidazoles, with a third further away.[63]

The characteristic frequencies at 0.97, 3.78, 4.86, and 5.46 MHz observed for [Cu(II)(TEPA)($^{14}NO_2$)]PF_6 and absent in the spectrum for [Cu(II)(TEPA)($^{15}NO_2$)]PF_6 (Figure 8B) are not observed in nitrite-treated hemocyanin. Both the 4.86- and 5.46-MHz lines arising from nitrite in the model are well separated from the frequencies attributed to the remote nitrogen of Cu(II)-coordinated histidine imidazole in the protein. Although the 4.86-MHz line for nitrite in the model has about a quarter of the intensity of the NQI lines for the remote ^{14}N of the coordinated imidazoles in the protein, it would clearly be observed were the

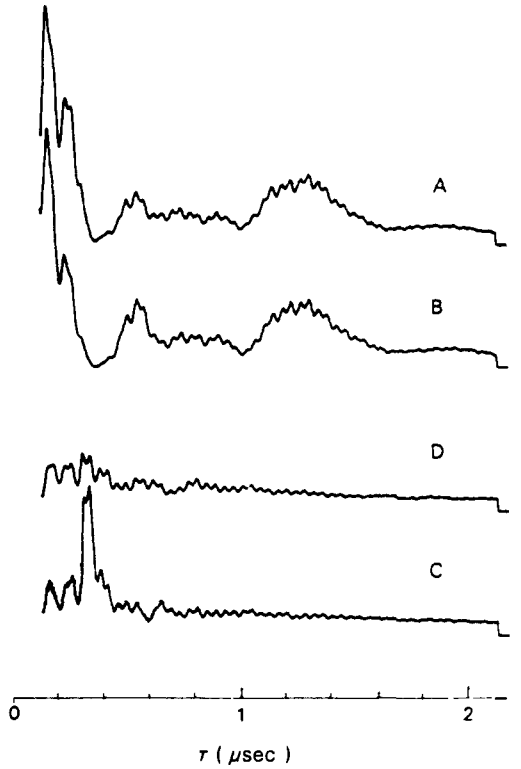

Figure 9. Two-pulse spin echo envelopes for (A) $^{14}NO_2^-$ and (B) $^{15}NO_2^-$ derivatives of hemocyanin and for **1** prepared with (C) $^{14}NO_2^-$ and (D) $^{15}NO_2^-$. Measurement conditions: microwave frequency, (A) 8.50 GHz, (B) 8.52 GHz, and (C and D) 8.55 GHz; magnetic field, (A and B) 2932 G, (C and D) 2981 G. Echo amplitudes of all four data sets were normalized to that of the $^{14}NO_2^-$ derivative of hemocyanin.

coupling between the nitrite nitrogen and the Cu(II) unpaired electron in the protein comparable to that in **1**.

The nitrite in **1** binds to Cu(II) primarily through one oxygen, with nitrogen uncoordinated. Were the nitrite to act as a bridging ligand in the protein, with one oxygen bound to Cu(II) and the nitrogen bound to Cu(I),[61] the electron population at the lone-pair orbital would be expected to decrease so that e^2qQ would decrease as well. The quadrupole frequencies would then be different from those in **1**. But, since the electron–nuclear coupling between the Cu(II) unpaired electron and the ^{14}N nucleus would likely be similar, the peak intensities in the ESEEM spectra should be comparable, about $^1/_4$ of that of the Cu(II)-coordinated histidine imidazoles. Were nitrite to act as a bridging ligand and bind to divalent copper equatorially through oxygen, a difference would be expected in the ESEEM spectra for $^{14}NO_2^-$- and $^{15}NO_2^-$-treated hemocyanin. None was found.

An alternative approach for demonstrating nitrite binding is to look for spectral differences in a two-pulse experiment between $^{14}NO_2^-$- and $^{15}NO_2^-$-treated hemocyanin. Two-pulse spin echo modulation studies have previously been used to demonstrate cyanide binding, on the basis of differences in nitrogen modulations for the Cu(II) protein galactose oxidase treated with either [^{14}N]- or [^{15}N]cyanide.[64] In this protein, Cu(II) is equatorially coordinated to two close imidazoles,[65] as in hemocyanin.[63] The ^{14}N of cyanide is separated from Cu(II) by a carbon atom, whereas the ^{14}N of the nitrite in the proposed structure for the nitrite derivative of hemocyanin is separated by an oxygen atom. The presence of $C^{14}N^-$ was recognized in the two-pulse spin echo envelope (ref 63, Figure 1D), even in the presence of deeper modulations arising from the two coordinated imidazoles.

The echo envelopes obtained by the two-pulse procedure for the [^{14}N]- and [^{15}N]nitrite products of hemocyanin are shown in Figure 9A,B, together with those for **1** prepared with $^{14}NO_2^-$

(62) McCracken, J.; Pember, S.; Benkovic, S. J.; Villafranca, J. J.; Peisach, J. *J. Am. Chem. Soc.* **1988**, *110*, 1069–1074.
(63) Gaykema, W. P. J.; Hol, W. G. J.; Vereijken, J. M.; Soeter, M. M.; Bal, H. J.; Beintema, J. J. *Nature (London)* **1984**, *309*, 23–29.
(64) Kosman, D. J.; Peisach, J.; Mims, W. B. *Biochemistry* **1980**, *19*, 1304–1308.
(65) Ito, N.; Yadav, K. D. S.; Knowles, P. F. *Nature* **1991**, *350*, 87–90.

and $^{15}NO_2^-$ (Figure 9C,D). The faster periodicity arises from ambient or weakly coupled protons while the slower periodicities arise from weakly coupled ^{14}N.[30] The differences observed between $^{14}NO_2^-$ and $^{15}NO_2^-$ of **1** are not found for the hemocyanin derivatives. Once again, there is no evidence that nitrite is equatorially coordinated to divalent copper through oxygen in the nitrite-treated protein.

This measurement, however, does not rule out the possibility that nitrite is axially coordinated to Cu(II). Axial coordination is expected to produce a smaller electron-nuclear coupling by roughly a factor of 30-50, by analogy with other Cu(II) complexes.[20,30,31] Therefore, nitrite that is axially coordinated to Cu(II) through oxygen would likely give rise to extremely shallow modulations because A_{iso} would be so much smaller than the electron-nuclear coupling and its spectral contribution would then not be distinguishable. Were nitrite to bind axially through nitrogen, its spectral contribution would be overwhelmed by those from coordinated imidazole nitrogens, and once again, not be recognized.

Conclusion. Nitrite binding in the model **1** is through oxygen, both in the crystalline state and in solution. The electron-nuclear coupling of ^{14}N and the unpaired electron of Cu(II) is comparable to the ^{14}N nuclear Zeeman interaction at X-band, and thus $^{14}NO_2^-$ modulations can be detected by ESEEM spectroscopy. The electron distribution on ^{14}N of Cu(II)-bound nitrite in frozen solution is very similar to that in solid, diamagnetic nitrite salts, as indicated from the quadrupole parameters (e^2qQ = 5.66 MHz, η = 0.31), suggesting similarities in metal-nitrite binding. This ESEEM investigation also suggests that in frozen solution the conformation of nitrite in **1** is the same as that in the crystal. The ESEEM study of nitrite-treated hemocyanin shows that nitrite does not coordinate to Cu(II) through oxygen as an equatorial ligand, as it does in the model.

Acknowledgment. This work was supported by NIH Grants RR-02583 and GM-40168 to J.P. and GM-45971 to K.D.K. We thank J. Zubieta and Q. Chen for a preliminary structural study of **1**.

Supplementary Material Available: Complete structure information including anisotropic thermal parameters for non-hydrogen atoms, atomic coordinates, and intramolecular distances and angles (12 pages); observed and calculated structure factors (29 pages). Ordering information is given on any current masthead page.

Lipidic Cubic Phases as Transparent, Rigid Matrices for the Direct Spectroscopic Study of Immobilized Membrane Proteins

Ehud M. Landau* and Pier Luigi Luisi

Contribution from the Institut für Polymere, ETH Zentrum, Universitätstrasse 6, CH-8092 Zürich, Switzerland. *Received September 9, 1992*

Abstract: Lipidic cubic phases composed of 1-palmitoyl-*sn*-glycero-3-phosphocholine and water were used as structured, transparent, rigid matrices in an attempt to develop novel media for simultaneous structural and functional investigations of membrane proteins. Bacteriorhodopsin and melittin, immobilized in the cubic phase, resulted in very stable materials, whose circular dichroism (CD) spectra exhibit contents of α-helicity akin to those expected from the crystal structures. As judged from CD, the native conformations were temperature independent in the range of existence of the cubic phase (0-50 °C). Addition of NaCl to the bacteriorhodopsin-containing cubic phase stabilized the binding of retinal to the immobilized protein. Without added salt, a slow (i.e., days long) dissociation of retinal at ambient conditions was observed, which however takes place without impairing the native protein's conformation.

Introduction

Compared to soluble proteins, our understanding of the structure-function relationship of membrane proteins is still quite rudimentary, due to the fact that membrane proteins carry out their specific functions when immobilized in their native environment—the membranes—and often undergo denaturation when extracted out of the membrane and solubilized. Moreover, very little structural information is available on membrane proteins, mainly due to the great technical difficulty in obtaining well diffracting crystals. An alternative approach—the use of electron microscopy for obtaining high-resolution structures—has only recently been successfully applied to bacteriorhodopsin.[1] In order to gain a better understanding of the structure-function relationship of membrane proteins, it would be necessary to perform both structural and functional studies in the immobilized state of the protein under conditions which mimic the native ones. We wish to report here on a class of materials—lipidic cubic phases—which exhibit a combination of useful properties, which render them very suitable for such studies.

Lipidic cubic phases, first described by Luzzati et al.,[2] are highly viscous, isotropic, and thermodynamically stable rigid materials composed of (phospho)lipids and water. Moreover, these materials are transparent, which makes them perfect matrices for spectroscopic investigations. Depending on the particular conditions and choice of lipids, different cubic structures can be formed. These are divided into two groups—bicontinuous and closed aggregates.[3] The bicontinuous group is based on a three-dimensional, curved bilayer structure of lipids surrounded by water, in which both components diffuse freely. The bilayer can be described by infinite periodic minimal surfaces, which have at each point a mean curvature of zero. The closed-aggregate group is built up of an ordered array of micelles, made up of diffusionally restricted lipids, surrounded by water. These remarkable properties should enable the immobilization and spectroscopic investigation of membrane species. Moreover, based on the fact that these materials are composed of crystallographically well-defined polar, nonpolar, and interfacial regions, we have anticipated that they

(1) Henderson, R.; Baldwin, J. M.; Ceska, T. A.; Zemlin, F.; Beckmann, E.; Downing, K. H. *J. Mol. Biol.* **1990**, *213*, 899.

(2) Luzzati, V.; Mustacchi, H.; Skoulios, A. *Disc. Faraday Soc.* **1958**, *25*, 43.

(3) (a) Lindblom, G.; Rilfors, L. *Biochim. Biophys. Acta* **1989**, *988*, 221. (b) Fontell, K. *Colloid Polym. Sci.* **1990**, *268*, 264.

0002-7863/93/1515-2102$04.00/0